Diviner Lunar Radiometer Observations of the LCROSS Impact

Paul O. Hayne,[1]* Benjamin T. Greenhagen,[2] Marc C. Foote,[2] Matthew A. Siegler,[1] Ashwin R. Vasavada,[2] David A. Paige[1]

The Lunar Reconnaissance Orbiter (LRO) Diviner instrument detected a thermal emission signature 90 seconds after the Lunar Crater Observation and Sensing Satellite (LCROSS) Centaur impact and on two subsequent orbits. The impact heated a region of 30 to 200 square meters to at least 950 kelvin, providing a sustained heat source for the sublimation of up to ~300 kilograms of water ice during the 4 minutes of LCROSS post-impact observations. Diviner visible observations constrain the mass of the sunlit ejecta column to be ~10^{-6} to 10^{-5} kilograms per square meter, which is consistent with LCROSS estimates used to derive the relative abundance of the ice within the regolith.

On 9 October 2009, the Diviner Lunar Radiometer onboard the Lunar Reconnaissance Orbiter (LRO) observed a controlled impact of the Lunar Crater Observation and Sensing Satellite (LCROSS) (*1*) into one of the coldest places on the Moon (*2*). Diviner's multispectral thermal infrared measurements of this event provide insight into energy dissipation and cooling during a planetary impact in a region where volatiles may be cold-trapped (*3*, *4*). We report on the effects of volatiles on the temperature behavior observed by Diviner and the LCROSS Shepherding Spacecraft (SSc).

Diviner is a push-broom visible and infrared radiometer with nine channels spanning wavelengths from 0.3 to 400 μm, with sensitivity to a broad range of temperatures (*5*) (table S1). Daytime brightness temperatures (Fig. 1B) show that the LCROSS impact site in Cabeus crater is in persistent shadow, with a nearly isothermal surface at ~40 K just before impact (*6*). Figure 1 shows that the LCROSS impact occurred near the center of one of the coldest regions of Cabeus crater. Thermal models (*2*) place the LCROSS impact site's annual average temperature at 37 K, in the 99.7th percentile (by area) for the region poleward of 80°S.

The LRO orbit was modified to put the closest approach (slant range 78 km) at 90 s after impact of the launch vehicle's spent Centaur upper stage, in order to better observe the LCROSS impact while protecting the spacecraft from debris. Also, the spacecraft was rolled 81.1° to allow the Lyman Alpha Mapping Project (LAMP) to view the lunar limb above Cabeus crater. Diviner

[1]Department of Earth and Space Sciences, University of California, Los Angeles, CA 90095, USA. [2]Jet Propulsion Laboratory, California Institute of Technology, Pasadena, CA 91109, USA.

*To whom correspondence should be addressed. E-mail: phayne@ucla.edu

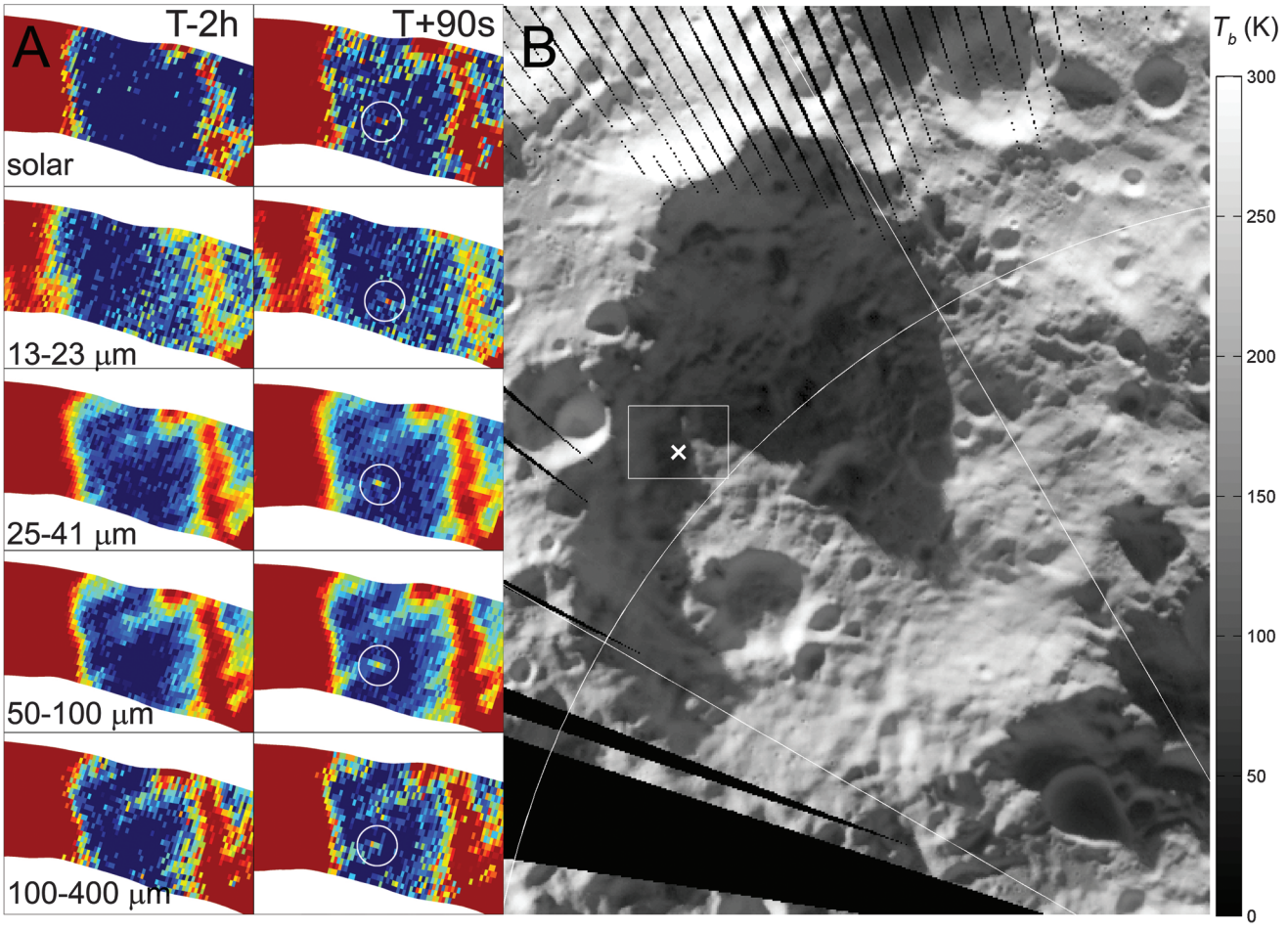

Fig. 1. (**A**) Pre- and post-impact images (T–2h, T+90s) of the LCROSS impact site. (**B**) Diviner 50- to 100-μm pre-impact brightness temperature map from nadir data, 1 to 15 October 2009. The width of each inset frame (white box) is about 15 km. The LCROSS impact site (x) had an estimated surface temperature of ~40 K just before impact (*6*). The colors for the solar channel scale linearly with radiance from 1.2×10^{-2} to 4.3×10^{-2} W m^{-2} sr^{-1}; the infrared frames are linear with brightness temperature, with ranges of 85 to 105 K (13 to 23 μm), 60 to 90 K (25 to 41 μm), 55 to 80 K (50 to 100 μm), and 65 to 80 K (100 to 400 μm).

has independent azimuth and elevation actuators, enabling targeted observations despite this unusual spacecraft attitude. Diviner targeted the impact site for eight orbits, separated by about 2 hours each, the third orbit occurring about 90 s after Centaur impact (T+90s). Diviner's view of the impact site was oblique, with an emission angle of ~48° and pixel size of ~400 m.

All seven of Diviner's infrared channels measured thermal emission from the Centaur impact crater during the T+90s observations (Fig. 1A). Also, the more sensitive of the two solar channels observed both thermal emission from the surface and scattered sunlight from the ejecta cloud. About 2 hours later, Diviner's three longest-wavelength channels again measured a thermal signal from the subpixel impact site. At 4 hours after impact (T+4h), only the channel spanning wavelengths of 25 to 41 μm measured a signal above the noise level. No signal due to the LCROSS Centaur impact was observed on later orbits. The complete set of measurements is summarized in table S1. This report focuses only on the Centaur impact, because emission from the SSc impact (which occurred after the T+90s observations and with much lower energy) has not yet been found in the data.

In addition to thermal emission from the Centaur impact site, we attribute an enhanced signal in Diviner's solar channel, evident over a broad (~140 km^2) region, to scattered sunlight from the ejecta plume. Using the radiance of the scattered sunlight, we calculate a total normal optical depth of 2.0×10^{-5} to 8.1×10^{-4} over this region at T+90s (*7*, *8*). Given a typical lunar soil grain size distribution (*9*), the total column mass is 1.0×10^{-6} to 4.1×10^{-5} kg m^{-2}. Assuming an even distribution over the 140-km^2 region, the total mass above the sunlight horizon of ~800 m is 2600^{+3200}_{-1400} kg (*10*). This range is consistent with those derived from the LCROSS spectrometer data (*1*), although some material may have been outside Diviner's field of view.

Thermal emission from the Centaur impact site at T+90s is dominated by near-surface material rapidly heated by friction during the impact (*11*). A simple model using two temperature components accurately reproduces the Diviner data, captures the primary features of the spectral energy distribution (figs. S2 and S4), and is generally consistent with SSc mid-infrared images of the impact site shortly after impact (*12*). In this model, dissipation generates a high-temperature component within the crater (diameter ~25 m) and a larger region with a somewhat lower temperature represents an ejecta blanket (diameter ~150 m).

We simulated radiance values for Diviner's spectral channels (table S1) by convolving each channel's spectral response with the area-weighted blackbody spectral radiance for each of the two temperature components, with a constant background radiance filling the remainder of the field of view. Diviner's high-sensitivity solar channel cannot detect temperatures below ~400 K for an area less than 10^3 m^2 (~1% pixel fill factor). Therefore, the clear thermal emission signal in this channel places a strong lower limit on the temperature of the hot component at T+90s. Using the 8-μm channels' T+90s radiances, we find a best-fit hot component temperature of 600^{+50}_{-90} K, with an area of 60^{+140}_{-30} m^2 (*6*, *13*).

Diviner's longer-wavelength infrared channels constrain the average ejecta blanket temperature to be 110^{+50}_{-20} K, with an area of $8.0^{+10}_{-6} \times 10^4$ m^2 at T+90s. Between ~0.5 and 1 km away from the impact, brightness temperatures are elevated slightly from the pre-impact background; this is attributed to emission by warm grains in the sunlit ejecta cloud. About 2 hours after the Centaur impact, the hot region had cooled below the ~450 K detection threshold (area 60 m^2) of the 8-μm channels. A χ^2 minimization procedure using the observed emission in two channels (25 to 41 μm and 50 to 100 μm) failed to yield a reliable best-fit temperature for the hot component; however, we estimate a mean temperature of ~100 K for the combined crater–ejecta blanket region. At T+4h, the 25- to 41-μm radiance was still above the background level, but the signal was too low to provide a compelling lower limit on temperature for either component.

Cooling of the impact zone occurred primarily by surface radiation to space, sublimation of ice, and (to a lesser degree) downward conduction at the base of the hot layer. We simulated these processes with a one-dimensional heat diffusion model, including the conductivity effects of ice as well as sublimation and vapor diffusion (*14*). An unknown fraction of the $\sim 7 \times 10^9$ J total impact energy is irreversibly converted to heat, although an upper limit of 20% is plausible (*15*, *16*). We investigated the cooling behavior of the hot inner region (30 to 200 m^2) for different values of E_h, the fraction of the total impact energy contributing to heating this zone (Fig. 2). Only cooling curves with E_h > 3% and initial temperature > 950 K are consistent with the T+90s observations; upper limits on these quantities are not well constrained (*6*). Ice within the regolith causes more rapid cooling by loss of latent and sensible heat, as well as more efficient downward conduction. If the regolith pores were filled with ice (50% porosity), we find that the heat energy fraction E_h must be >12%, otherwise cooling is too rapid to match the T+90s Diviner data. Conversely, if E_h = 5%, ice mass fractions must be <4%. Thus, an independent constraint on E_h would effectively place limits on the initial ice content in the impact zone.

Diviner's estimate for the area of the hot component, 30 to 200 m^2, is somewhat less than the area of the Centaur's impact crater, ~500 to 700 m^2 (*12*), which indicates that some portion of this region cooled below the detection limit of ~300 K (for an area of 500 m^2) of the Diviner 8-μm channels in less than 90 s. This is consistent with SSc NIR2 images of the Centaur crater about 4 min after impact, which reveal a dark inner region, perhaps due to more rapid cooling of icy material at depth (*12*). An increase in ice content of just a few percent by mass over the excavation depth (~1 to 3 m) could result in more than 100 K of cooling within the crater relative to the rim after 250 s (Fig. 2), in which case the crater floor should appear darker in emission. A conservative upper limit on the crater floor temperature of 410 K at 250 s after

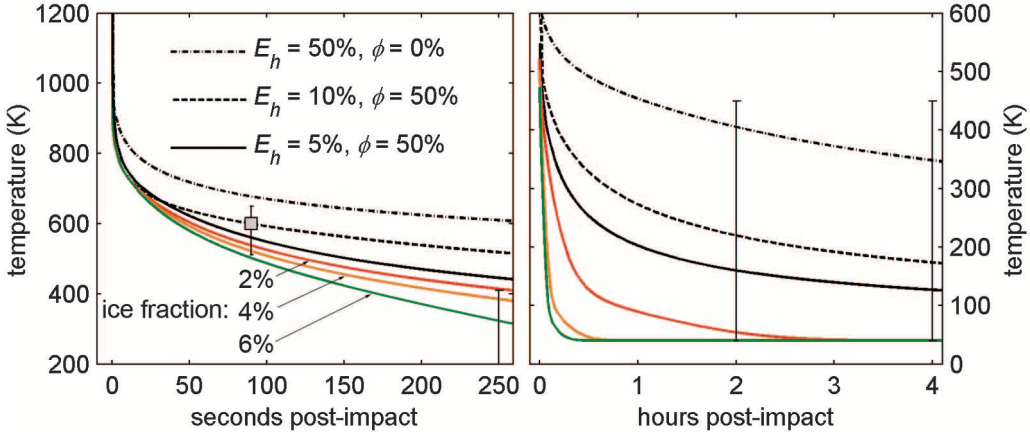

Fig. 2. Modeled cooling curves for a 60-m^2 region of porosity ϕ heated by a fraction E_h of the total impact kinetic energy. The initial temperature is a free parameter, as is the ice content in the regolith, both of which determine the initial depth of heating (typically a few millimeters) for a given value of E_h. The data point at 90 s after impact is from Diviner data; the upper limit of 410 K at 250 s after impact refers to the dark crater observed by the LCROSS SSc (*12*, *17*). Upper limits at T+2h and T+4h are based on Diviner thermal observations. If ice content increases with depth, interior parts of the crater should follow the steepest cooling curves. Note that the ice mass fraction (plotted for E_h = 5%) can only be constrained for a given value of E_h.

impact can be derived from the relative brightness of the surrounding terrain observed by both NIR2 and Diviner (*17*). Model cooling curves for E_h = 5% (Fig. 2) show that a regolith ice mass fraction of >2% is required to reproduce this behavior for the assumed regolith properties.

Finally, a layer a few millimeters thick heated to an initial temperature of ~1000 K is consistent with both the Diviner data and the dynamics of the hydrogen vapor cloud observed by LAMP (*18*). At these temperatures, the regolith is desiccated nearly instantaneously, but a more gradual flux of sublimed water molecules continues as the thermal wave propagates downward. The above models imply that this gradual process accounts for ~30% of water molecules sublimed within the impact zone over the course of 4 min. For a heated area of 30 to 200 m^2 and ice mass fractions of 1%, 10%, and 22% (filled pores), instantaneous and gradual sublimation produce a total of 3 to 20 kg, 20 to 130 kg, and 50 to 300 kg of water vapor, respectively. This range is comparable to the ~155 kg of water vapor observed by LCROSS during this period (*1*). Thus, a substantial portion of the observed water vapor may have been supplied by the steaming crater.

References and Notes

1. A. Colaprete *et al.*, *Science* **330**, 463 (2010).
2. D. A. Paige *et al.*, *Science* **330**, 479 (2010).
3. K. Watson, B. C. Murray, H. Brown, *J. Geophys. Res.* **66**, 3033 (1961).
4. J. A. Zhang, D. A. Paige, *Geophys. Res. Lett.* **36**, L16203 (2009).
5. D. A. Paige *et al.*, *Space Sci. Rev.* **150**, 125 (2010).
6. See supporting material on *Science* Online.
7. Optical depth was calculated from the difference in counts between the T+90s orbit and the average of the T–2h and T+2h orbits (*6*), converted to radiance using a factor of 3.9 (±10%) × 10^{-3} W m^{-2} sr^{-1} $counts^{-1}$. Assuming single scattering, the total normal optical depth is $\tau = (4\pi/\mu)/(F\varpi_0 P)$, where I is the measured radiance enhancement, μ is the emission angle cosine, F is the solar irradiance within the pass band (1130 W m^{-2}), $\varpi_0 \approx 0.34$ is the single-scattering albedo, and $P \approx 0.38$ is the scattering phase function for lunar soil (*8*). The measurement error in the solar channel is estimated to be ~2 counts, giving an uncertainty of 2.8 counts (~0.01 W m^{-2} sr^{-1}) in the difference.
8. E. J. Foote *et al.*, *40th Lunar Planet. Sci. Conf.*, abstract 2500 (2009).
9. W. D. Carrier, *Moon* **6**, 250 (1973).
10. We calculated the second and third moments of a lunar soil size distribution (*9*), giving corresponding radii $r_2 \approx 13$ μm (cross section–weighted mean) and $r_3 \approx 16$ μm (volume-weighted mean). The column mass (kg m^{-2}) was then calculated according to $\mu = \frac{4}{3}\pi\rho r_3^3 \cdot N = \frac{4}{3}\rho r_3^3 \tau / Q_{ext} r_2^2$, where ρ = 3600 kg m^{-3} is the density of individual grains, τ is the visible optical depth, and Q_{ext} = 2.0 is the optical extinction efficiency.
11. G. V. Belyakov *et al.*, *Combust. Explos. Shock Waves* **13**, 524 (1977).
12. P. H. Schultz *et al.*, *Science* **330**, 468 (2010).
13. The ranges account for the combined 1σ measurement error in all channels due to instrument noise, data misregistration, background variability, and field-of-view effects (*6*).
14. The 1D thermal model is based on that of Vasavada *et al.* (*19*) and includes vertical conduction and surface emission as well as temperature-dependent thermal conductivities and heat capacities. Our ice sublimation and vapor diffusion model is based on that of Fanale and Salvail (*20*) for comets, where we have adapted the thermal model to adjust thermophysical properties according to local ice content. Unless otherwise indicated, we assume a porosity of 50%, mean grain separation of 70 μm, and infrared emissivity of 0.95.
15. D. Braslau, *J. Geophys. Res.* **75**, 3987 (1970).
16. D. E. Rehfuss, *Moon* **11**, 19 (1974).
17. Topographic features illuminated by indirect sunlight around the shadowed impact site cannot be clearly seen in Diviner's pre-impact solar channel data, although these features are observed by the LCROSS near-infrared camera (NIR2) (*12*). Because the indirect sunlight signal is below Diviner's noise level of 2 counts in the solar channel, the upper limit of this signal is ~2× the gain factor, or I_{Div} = 7.8 × 10^{-3} W m^{-2} sr^{-1}. The radiance actually observed by NIR2 for such a signal is less than $I_{NIR} = (I_{Div}/F_{Div}) \cdot F_{NIR}$, where F is the solar irradiance at the Moon for the given pass band. Although the value of F_{NIR} is unknown, we estimate it to be 130 W m^{-2}, assuming 80% sensitivity from 1000 to 1700 nm and zero sensitivity outside this range (*21*). Again using F_{Div} = 1130 W m^{-2}, this yields I_{NIR} = 0.9 × 10^{-3} W m^{-2} sr^{-1}. Setting this equal to the equivalent blackbody radiance for the same pass band gives a value of ~410 K as a conservative estimate of NIR2's minimum detectable temperature.
18. G. R. Gladstone *et al.*, *Science* **330**, 472 (2010).
19. A. R. Vasavada, D. A. Paige, S. Wood, *Icarus* **141**, 179 (1999).
20. F. P. Fanale, J. R. Salvail, *Icarus* **60**, 476 (1984).
21. Goodrich SU320KTX-1.7RT (spec sheet, www.sensorsinc.com/downloads/SU320KTX.pdf).

22. Some of the research described in this paper was carried out at the Jet Propulsion Laboratory, California Institute of Technology, under a contract with NASA.

Supporting Online Material

www.sciencemag.org/cgi/content/full/330/6003/477/DC1
Materials and Methods
Figs. S1 to S8
Table S1
References

30 August 2010; accepted 22 September 2010
10.1126/science.1197135

Diviner Lunar Radiometer Observations of Cold Traps in the Moon's South Polar Region

David A. Paige,[1*] Matthew A. Siegler,[1] Jo Ann Zhang,[1] Paul O. Hayne,[1] Emily J. Foote,[1] Kristen A. Bennett,[1] Ashwin R. Vasavada,[2] Benjamin T. Greenhagen,[2] John T. Schofield,[2] Daniel J. McCleese,[2] Marc C. Foote,[2] Eric DeJong,[2] Bruce G. Bills,[2] Wayne Hartford,[2] Bruce C. Murray,[3] Carlton C. Allen,[4] Kelly Snook,[5] Laurence A. Soderblom,[6] Simon Calcutt,[7] Fredric W. Taylor,[7] Neil E. Bowles,[7] Joshua L. Bandfield,[8] Richard Elphic,[9] Rebecca Ghent,[10] Timothy D. Glotch,[11] Michael B. Wyatt,[12] Paul G. Lucey[13]

Diviner Lunar Radiometer Experiment surface-temperature maps reveal the existence of widespread surface and near-surface cryogenic regions that extend beyond the boundaries of persistent shadow. The Lunar Crater Observation and Sensing Satellite (LCROSS) struck one of the coldest of these regions, where subsurface temperatures are estimated to be 38 kelvin. Large areas of the lunar polar regions are currently cold enough to cold-trap water ice as well as a range of both more volatile and less volatile species. The diverse mixture of water and high-volatility compounds detected in the LCROSS ejecta plume is strong evidence for the impact delivery and cold-trapping of volatiles derived from primitive outer solar system bodies.

The Moon's polar regions are notable because of their potential to cryogenically trap water ice and other volatile species (*1*). The Lunar Reconnaissance Orbiter (*2*) (LRO) Diviner Lunar Radiometer Experiment has been mapping the infrared emission from the Moon since July 2009 using seven spectral channels that span a wavelength range from 7.55 to 400 μm at a spatial resolution of ~200 m (*3*). Thermal maps of the south polar region (Fig. 1, A and B) were obtained during the LRO monthly mapping cycle just before the Lunar Crater Observation and Sensing Satellite (LCROSS) impact (*4*), as the Moon approached southern summer solstice (*5*). The mapped quantity is the bolometric brightness temperature, which is the wavelength-integrated radiance in all seven Diviner channels expressed as the temperature of an equivalent blackbody (*6*). For quantifying the overall heat balance of the surface and comparing with available models, the bolometric brightness temperature is the most fundamental and interpretable measurable quantity. For the simplest case in which Diviner's surface footprint is filled with a blackbody of uniform surface temperature, the bolometric brightness temperature will be equal to the temperature of the surface. In the more general case, where Diviner's surface

[1]Department of Earth and Space Sciences, University of California, Los Angeles, 595 Charles E. Young Drive East, Los Angeles, CA 90095, USA. [2]Jet Propulsion Laboratory, California Institute of Technology, Pasadena, CA 91109, USA. [3]California Institute of Technology, Pasadena, CA 90025, USA. [4]NASA Johnson Space Center, Houston, TX 77058, USA. [5]NASA Goddard Space Flight Center, Greenbelt, MD 20771, USA. [6]U.S. Geological Survey, Flagstaff, AZ 86001, USA. [7]Oxford University, Oxford OX1 3PU, UK. [8]University of Washington, Seattle, WA 98195, USA. [9]NASA Ames Research Center, Moffett Field, CA 94035, USA. [10]University of Toronto, Toronto, ON M5S 3B1, Canada. [11]State University of New York, Stony Brook, NY 11794, USA. [12]Brown University, Providence, RI 02912, USA. [13]University of Hawaii, Honolulu, HI 96822, USA.

*To whom correspondence should be addressed. E-mail: dap@moon.ucla.edu

Science

Diviner Lunar Radiometer Observations of the LCROSS Impact

Paul O. Hayne, Benjamin T. Greenhagen, Marc C. Foote, Matthew A. Siegler, Ashwin R. Vasavada and David A. Paige

Science **330** (6003), 477-479.
DOI: 10.1126/science.1197135

Watering the Moon

About a year ago, a spent upper stage of an Atlas rocket was deliberately crashed into a crater at the south pole of the Moon, ejecting a plume of debris, dust, and vapor. The goal of this event, the Lunar Crater Observation and Sensing Satellite (LCROSS) experiment, was to search for water and other volatiles in the soil of one of the coldest places on the Moon: the permanently shadowed region within the Cabeus crater. Using ultraviolet, visible, and near-infrared spectroscopy data from accompanying craft, **Colaprete *et al.*** (p. 463; see the news story by **Kerr**; see the cover) found evidence for the presence of water and other volatiles within the ejecta cloud. **Schultz *et al.*** (p. 468) monitored the different stages of the impact and the resulting plume. **Gladstone *et al.*** (p. 472), using an ultraviolet spectrograph onboard the Lunar Reconnaissance Orbiter (LRO), detected H_2, CO, Ca, Hg, and Mg in the impact plume, and **Hayne *et al.*** (p. 477) measured the thermal signature of the impact and discovered that it had heated a 30 to 200 square-meter region from ~40 kelvin to at least 950 kelvin. **Paige *et al.*** (p. 479) mapped cryogenic zones predictive of volatile entrapment, and **Mitrofanov *et al.*** (p. 483) used LRO instruments to confirm that surface temperatures in the south polar region persist even in sunlight. In all, about 155 kilograms of water vapor was emitted during the impact; meanwhile, the LRO continues to orbit the Moon, sending back a stream of data to help us understand the evolution of its complex surface structures.